Lee et al. Nanoscale Research Letters (2016) 11:433
DOI 10.1186/s11671-016-1637-9

Nanoscale Research Letters

NANO EXPRESS Open Access

Tunneling-Magnetoresistance Ratio Comparison of MgO-Based Perpendicular-Magnetic-Tunneling-Junction Spin Valve Between Top and Bottom $Co_2Fe_6B_2$ Free Layer Structure

Du-Yeong Lee, Seung-Eun Lee, Tae-Hun Shim and Jea-Gun Park*

Abstract

For the perpendicular-magnetic-tunneling-junction (p-MTJ) spin valve with a nanoscale-thick bottom $Co_2Fe_6B_2$ free layer ex situ annealed at 400 °C, which has been used as a common p-MTJ structure, the Pt atoms of the Pt buffer layer diffused into the MgO tunneling barrier. This transformed the MgO tunneling barrier from a body-centered cubic (b.c.c) crystallized layer into a mixture of b.c.c, face-centered cubic, and amorphous layers and rapidly decreased the tunneling-magnetoresistance (TMR) ratio. The p-MTJ spin valve with a nanoscale-thick top $Co_2Fe_6B_2$ free layer could prevent the Pt atoms diffusing into the MgO tunneling barrier during ex situ annealing at 400 °C because of non-necessity of a Pt buffer layer, demonstrating the TMR ratio of ~143 %.

Keywords: p-MTJ, BEOL, TMR ratio, Pt diffusion, Top and bottom free layer

Background

Perpendicular spin-transfer-torque magnetic random access memory (p-STT MRAM) has recently been greatly researched because it would overcome the scaling-down limitation of less than 10 nm of current dynamic random access memory (DRAM) [1, 2]. To achieve a tera-bit integration memory cell, three critical device performance parameters of CoFeB/MgO-based perpendicular-magnetic-tunneling-junction (p-MTJ) spin valves in a p-STT MRAM cell have been rapidly improved: tunneling-magnetoresistance (TMR) ratio, thermal stability (Δ), and switching current density (J_c) [3–6]. In particular, the structure design of a p-MTJ spin valve (i.e., a p-MTJ spin valve with a nanoscale-thick top free layer or a p-MTJ spin valve with a nanoscale-thick bottom free layer) has intensively been studied to achieve a higher TMR ratio at the back end of line (BEOL) temperature of 400 °C [7–10]. Note that the BEOL temperature of 400 °C is required to integrate memory cells [11]. In addition, for a p-MTJ spin valve with a nanoscale-thick top free layer, the CoFeB free layer is located above the synthetic antiferromagnetic (SyAF) layer in a p-MTJ spin valve, while for a p-MTJ spin valve with a nanoscale-thick bottom free layer, the CoFeB free layer is located below the SyAF layer in a p-MTJ spin valve. In our study, the dependencies of the TMR ratio at the BEOL temperatures of 350 and 400 °C on the structure of a p-MTJ spin valve were investigated. In addition, the reason the structure difference for a p-MTJ spin valve directly influences the TMR ratio was characterized by static magnetization behavior, crystallinity, and the depth profile of atomic composition of p-MTJ spin valves.

Methods

CoFeB/MgO-based p-MTJ spin valves with a $[Co/Pt]_n$-based SyAF layer were prepared using a 12-in. multi-chamber sputtering system under a high vacuum of less than 1×10^{-8} torr without breaking vacuum. Two types of p-MTJ spin valves were fabricated on 12-in. SiO_2 wafers, as shown in Fig. 1: One type was a p-MTJ spin valve with a bottom $Co_2Fe_6B_2$ free layer and the other type was a p-MTJ spin valve with a top $Co_2Fe_6B_2$ free layer.

* Correspondence: parkjgL@hanyang.ac.kr
Department of Electronics and Computer Engineering, Hanyang University, Seoul 04763, Republic of Korea

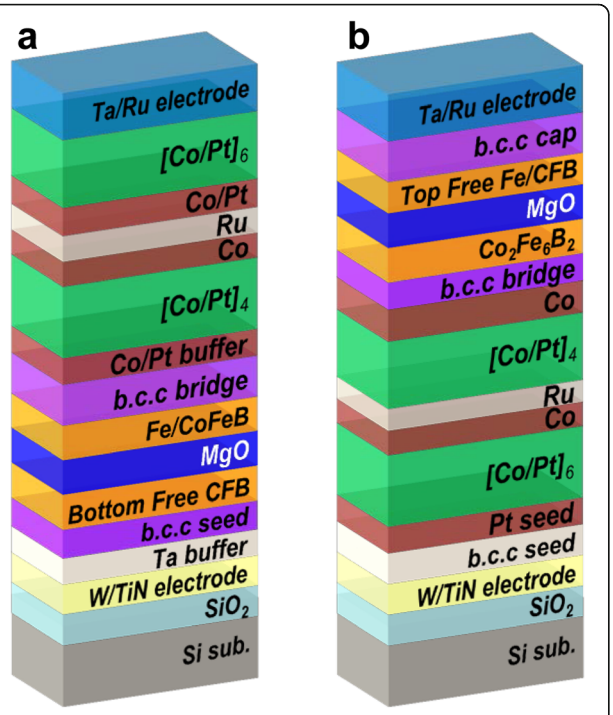

Fig. 1 p-MTJ spin valve structure. **a** p-MTJ spin valve with a nanoscale-thick bottom $Co_2Fe_6B_2$ free layer. **b** p-MTJ spin valve with a nanoscale-thick top $Co_2Fe_6B_2$ free layer

As shown in Fig. 1a, p-MTJ spin valves with a bottom $Co_2Fe_6B_2$ free layer were deposited with vertically stacked layers from the SiO_2 substrate, W/TiN bottom electrode/Ta buffer layer/body-centered-cubic (b.c.c) seed layer/$Co_2Fe_6B_2$ (1.0 nm) free layer/MgO (1.15 nm) tunnel barrier/Fe (0.4 nm)/$Co_2Fe_6B_2$ (1.0 nm) pinned layer/b.c.c bridge layer/Co/Pt (2.0 nm) buffer layer/lower $[Co/Pt]_4$-SyAF layer/Co/Ru spacer/Co/Pt/upper $[Co/Pt]_6$-SyAF layer/Ta/Ru top electrode. On the other hand, as shown in Fig. 1b, p-MTJ spin valves with a top $Co_2Fe_6B_2$ free layer were deposited with vertically stacked layers from the SiO_2 substrate, W/TiN bottom electrode/Ta buffer layer/Pt (3.0 nm) seed layer/upper $[Co/Pt]_6$-SyAF layer/Co/Ru spacer/Co/Pt/lower $[Co/Pt]_4$-SyAF layer/Co/b.c.c bridge layer/$Co_2Fe_6B_2$ (1.0 nm) pinned layer/MgO (1.15 nm) tunnel barrier/Fe (0.4 nm)/$Co_2Fe_6B_2$ (1.0 nm) free layer/b.c.c capping layer/Ta/Ru top electrode. The b.c.c metal has a lattice constant of 3.16 Å [3]. In addition, a 0.4-nm-thick Fe layer was inserted between the MgO tunneling barrier and the $Co_2Fe_6B_2$ layer to obtain a higher TMR ratio [12]. All p-MTJ spin valves were subject to ex situ annealing at 350 or 400 °C under a perpendicular magnetic field of 3 T.

Results and Discussion

The TMR ratio for p-MTJ spin valves depending on the p-MTJ spin valve structure was estimated by using current-in-plane tunneling (CIPT) at room temperature [13], as shown in Fig. 2. At an ex situ annealing temperature of 350 °C, the TMR ratio was ~160 % for the p-MTJ spin valve with a nanoscale-thick bottom $Co_2Fe_6B_2$ free layer and ~158 % for the p-MTJ spin valve with a nanoscale-thick top $Co_2Fe_6B_2$ free layer, indicating the TMR ratio did not depend on the p-MTJ spin valve structure. However, the TMR ratio for the p-MTJ spin valve with a nanoscale-thick bottom $Co_2Fe_6B_2$ free layer rapidly decreased from ~160 to ~72 % when the ex situ annealing temperature increased from 350 to 400 °C. Otherwise, the TMR ratio for the p-MTJ spin valve with a nanoscale-thick top $Co_2Fe_6B_2$ free layer slightly decreased from ~158 to ~143 % when the ex situ annealing temperature increased from 350 to 400 °C. These results imply that the TMR ratio for the p-MTJ spin valve with a nanoscale-thick bottom $Co_2Fe_6B_2$ free layer (~88 %) decreased by approximately six more than that for the p-MTJ spin valve with a nanoscale-thick top $Co_2Fe_6B_2$ free layer (~15 %).

First, to reveal the reason the TMR ratio at an ex situ annealing temperature of 400 °C depends on the p-MTJ spin valve structure, the dependency of the static magnetization behavior of p-MTJ spin valves on the p-MTJ spin valve structure was investigated via the magnetic moment vs. magnetic field (*M-H*) curves measured by a vibrating sampling magnetometer (VSM) at room temperature, as shown in Fig. 3. Both p-MTJ spin valves with nanoscale-thick bottom and top $Co_2Fe_6B_2$ free layers consisted of four magnetic layers as shown in Fig. 3a, b: $Co_2Fe_6B_2$ free layer (a), $Co_2Fe_6B_2$ pinned layer (b), lower SyAF layer (c), and upper SyAF layer (d). In Fig. 3, the length of boxes and vectors corresponds to

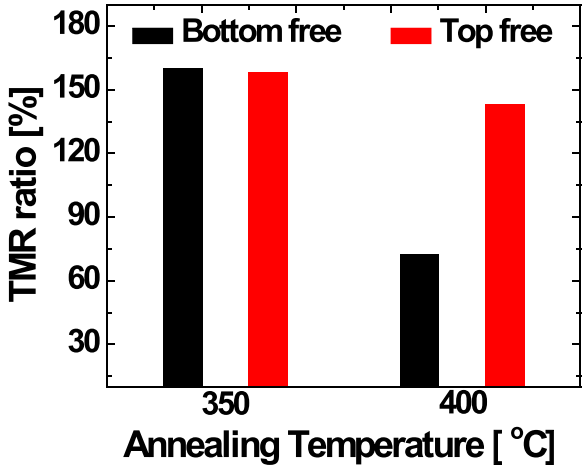

Fig. 2 TMR ratio depending on the p-MTJ spin valve structure and ex situ annealing temperature. (*Black*) p-MTJ spin valve with a nanoscale-thick bottom $Co_2Fe_6B_2$ free layer and (*red*) p-MTJ spin valve with a nanoscale-thick top $Co_2Fe_6B_2$ free layer ex situ annealed at 350 and 400 °C

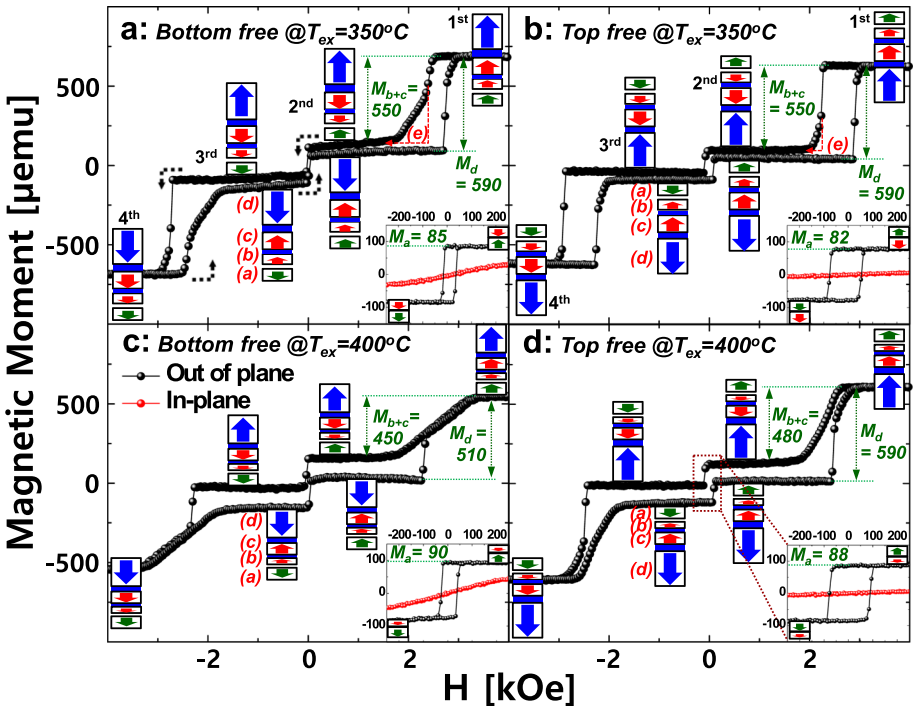

Fig. 3 Dependency of *M-H* curves on the p-MTJ spin valve structure and ex situ annealing temperature. *M-H* curves in figures describe the static perpendicular magnetization behaviors of $Co_2Fe_6B_2$ free layer (**a**), $Co_2Fe_6B_2$ pinned layer (**b**), lower SyAF layer (**c**), and upper SyAF layer (**d**). *M-H* curves in the inlets of figures only correspond to the static i-PMA behavior of $Co_2Fe_6B_2$ free layer, where the *black M-H* curves represent i-PMA behavior and the *red M-H* curves represent the in-plane behavior. **a** p-MTJ spin valve with a nanoscale-thick bottom $Co_2Fe_6B_2$ free layer ex situ annealed at 350 °C, **b** p-MTJ spin valve with a nanoscale-thick top $Co_2Fe_6B_2$ free layer ex situ annealed at 350 °C, **c** p-MTJ spin valve with a nanoscale-thick bottom $Co_2Fe_6B_2$ free layer ex situ annealed at 400 °C, and **d** p-MTJ spin valve with a nanoscale-thick top $Co_2Fe_6B_2$ free layer ex situ annealed at 400 °C

the magnitude of magnetic moment and the spin-electron direction for a magnetic layer, respectively. Initially, the $Co_2Fe_6B_2$ pinned layer (b) was ferro-coupled with the lower SyAF layer (c) while the lower SyAF layer (c) was antiferro-coupled with the upper SyAF layer (d) [14, 15]. Thus, when the applied magnetic field is scanned from 0, 300, 0, −300, and 0 Oe, only the spin-electron direction of the $Co_2Fe_6B_2$ free layer (a) can be rotated along the applied magnetic field direction, as shown in the inlets in Fig. 3. However, when the applied magnetic field is scanned from 0, 3, 0, −3, and 0 kOe, the spin-electron directions of all four magnetic layers can be rotated. For the p-MTJ spin valve with a nanoscale-thick bottom $Co_2Fe_6B_2$ free layer ex situ annealed at 350 °C, the magnetic moments of the $Co_2Fe_6B_2$ free layer (a), $Co_2Fe_6B_2$ pinned layer ferro-coupled with lower SyAF layer (b + c), and upper SyAF layer (d) were 85, 550, and 590 μemu, respectively, as shown in Fig. 3a. In addition, the nanoscale-thick bottom $Co_2Fe_6B_2$ free layer showed an excellent interface-perpendicular-magnetic-anisotropy (i-PMA) characteristic [16, 17], as shown in the *M-H* curve of the bottom $Co_2Fe_6B_2$ free layer in the inlet in Fig. 3a. On the other hand, for the p-MTJ spin valve with a nanoscale-thick top $Co_2Fe_6B_2$ free layer ex situ annealed at 350 °C, the magnetic moments of the $Co_2Fe_6B_2$ free layer (a), $Co_2Fe_6B_2$ pinned layer ferro-coupled with lower SyAF layer (b + c), and upper SyAF layer (d) were 82, 550, and 590 μemu, respectively, as shown in Fig. 3b. In addition, the top $Co_2Fe_6B_2$ free layer showed an excellent i-PMA characteristic, as shown in the *M-H* curve of the top $Co_2Fe_6B_2$ free layer in the inlet in Fig. 3b. The magnetic moments for the p-MTJ spin valves with a nanoscale-thick bottom $Co_2Fe_6B_2$ free layer and a top $Co_2Fe_6B_2$free layer were almost the same, indicating that these p-MTJ spin valves did not significantly differ in terms of static magnetic behavior except a slight degradation in the ferro-coupling strength between the $Co_2Fe_6B_2$ pinned layer ferro-coupled with the lower SyAF layer (compare (e) in Fig. 3a with (e) in Fig. 3b). However, for the p-MTJ spin valve with a nanoscale-thick bottom $Co_2Fe_6B_2$ free layer, when the ex situ annealing temperature increased from 350 to 400 °C, the magnetic moment of the bottom $Co_2Fe_6B_2$ free layer (see the inlets of Fig. 3a, c) slightly increased from 85 to 90 μemu while that of the $Co_2Fe_6B_2$ pinned layer ferro-coupled with lower SyAF layer (see (b + c) of Fig. 3a, c) decreased from 550 to 450 μemu and that of the upper SyAF layer (see (d) of Fig. 3a, c) decreased from 590 to 510 μemu. These results indicate that i-PMA

characteristic (PMA magnetic moment) of the $Co_2Fe_6B_2$ pinned layer for the p-MTJ spin valve with a nanoscale-thick bottom $Co_2Fe_6B_2$ free layer was remarkably degraded when the ex situ annealing temperature increased from 350 to 400 °C. Furthermore, for the p-MTJ spin valve with a nanoscale-thick top $Co_2Fe_6B_2$ free layer, when the ex situ annealing temperature increased from 350 to 400 °C, the magnetic moments increased slightly from 82 to 88 μemu for the top $Co_2Fe_6B_2$ free layer (see the inlets of Fig. 3b, d) but decreased from 550 to 480 μemu for the $Co_2Fe_6B_2$ pinned layer ferro-coupled with the lower SyAF layer (see (b + c) of Fig. 3b, d) and at stayed at 590 μemu for the upper SyAF layer (see (d) of Fig. 3c, d). These results imply that i-PMA characteristic (i.e., PMA magnetic moment) slightly degraded for the $Co_2Fe_6B_2$ pinned layer for the p-MTJ spin valve with a nanoscale-thick top $Co_2Fe_6B_2$ free layer but barely changed for the SyAF layer. In summary, when the ex situ annealing temperature increased from 350 to 400 °C, i-PMA characteristic degradation (i.e., PMA magnetic moment decrease) of the $Co_2Fe_6B_2$ pinned layer was much severer for the p-MTJ spin valve with a nanoscale-thick bottom $Co_2Fe_6B_2$ free layer than the p-MTJ spin valve with a nanoscale-thick top $Co_2Fe_6B_2$ free layer.

Since the TMR ratio for the p-MTJ spin valves is mainly determined by the i-PMA characteristic (i.e., PMA magnetic moment) of the $Co_2Fe_6B_2$ pinned layer as well as the b.c.c crystallinity of the MgO tunneling barrier, when the ex situ annealing temperature increased from 350 to 400 °C, the dependency of the MgO tunneling barrier b.c.c crystallinity on the p-MTJ structure (i.e., the p-MTJ with a nanoscale-thick bottom or top $Co_2Fe_6B_2$ free layer) was investigated as a function of ex situ annealing temperature via cross-sectional transmission electron microscope (x-TEM) observation, as shown in Fig. 4. For the p-MTJ spin valve with a nanoscale-thick bottom $Co_2Fe_6B_2$ free layer ex situ annealed at 350 °C, the $Co_2Fe_6B_2$ pinned layer and the MgO tunneling barrier were revealed as an amorphous layer ((a) in Fig. 4a) and a (100) b.c.c crystallized layer ((b) in Fig. 4a) [18–20], respectively. In particular, the MgO tunneling barrier was flatly grown, and the thickness of the MgO tunneling barrier was very uniform. In addition, for the p-MTJ spin valve with a nanoscale-thick top $Co_2Fe_6B_2$ free layer ex situ annealed at 350 °C, the $Co_2Fe_6B_2$ pinned layer and the MgO tunneling barrier were also exhibited as an amorphous layer ((a) in Fig. 4b) and (100) b.c.c crystallized layer ((b) in Fig. 4b), respectively. Surprisingly, the MgO tunneling barrier was flexuously grown although the thickness of the MgO tunneling barrier was almost uniform. Note that a flexuous growth of the MgO tunneling barrier in Fig. 4b originated from a thick SyAF layer and could degrade the b.c.c crystallinity of the MgO tunneling barrier. Otherwise, for the p-MTJ spin valve with a nanoscale-thick bottom $Co_2Fe_6B_2$ free layer, when the ex situ annealing temperature increased from 350 to 400 °C, the $Co_2Fe_6B_2$ pinned layer was revealed as a (100) b.c.c crystallized layer because of the texturing of the b.c.c bridging layer during ex situ annealing at 400 °C ((a) in Fig. 4c) rather than an amorphous layer, and the MgO tunneling barrier was exposed as a mixture of (100) b.c.c crystallized ((b) in Fig. 4c), (111) f.c.c crystallized ((c) in Fig. 4c) [21–24], and amorphous layers ((d) in Fig. 4c). In particular, this b.c.c crystallinity degradation (i.e., a mixture of b.c.c, f.c.c crystallized, and amorphous layers) would abruptly reduce the TMR ratio of the p-MTJ since it leads to a rapid decrease in Δ1 coherent tunneling of the MgO tunneling barrier [25–29]. Furthermore, for the p-MTJ spin valve with a nanoscale-thick top $Co_2Fe_6B_2$

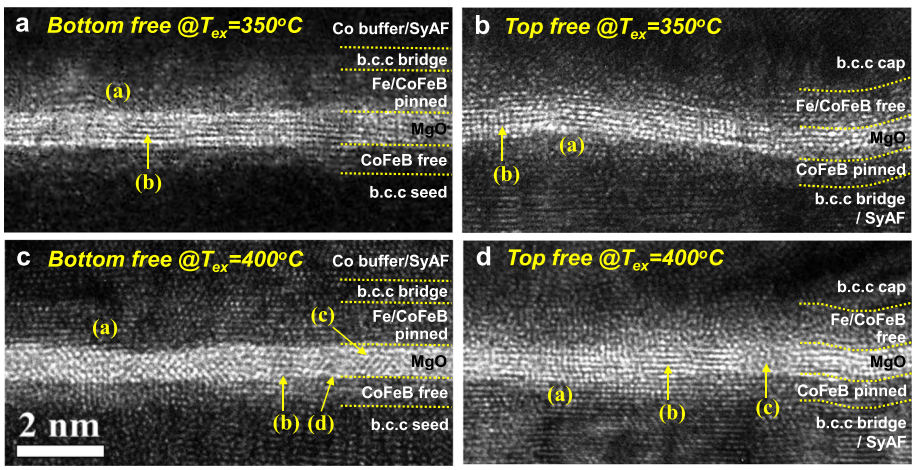

Fig. 4 Dependency of MgO tunneling crystallinity on the p-MTJ spin valve structure and ex situ annealing temperature. **a** p-MTJ spin valve with a nanoscale-thick bottom $Co_2Fe_6B_2$ free layer ex situ annealed at 350 °C, **b** p-MTJ spin valve with a nanoscale-thick top $Co_2Fe_6B_2$ free layer ex situ annealed at 350 °C, **c** p-MTJ spin valve with a nanoscale-thick bottom $Co_2Fe_6B_2$ free layer ex situ annealed at 400 °C, and **d** p-MTJ spin valve with a nanoscale-thick top $Co_2Fe_6B_2$ free layer ex situ annealed at 400 °C

free layer, when the ex situ annealing temperature increased from 350 to 400 °C, the $Co_2Fe_6B_2$ pinned layer was delineated as a b.c.c crystallized layer due to the texturing of the b.c.c bridging layer during ex situ annealing at 400 °C ((a) in Fig. 4d). The MgO tunneling barrier was also exposed as a b.c.c crystallized layer ((b) in Fig. 4d) including a local amorphous layer ((c) in Fig. 4d) and was flexuously grown. In summary, when the ex situ annealing temperature increased from 350 to 400 °C, the b.c.c crystallinity of the MgO tunneling barrier rapidly degraded for the p-MTJ spin valve with a nanoscale-thick bottom $Co_2Fe_6B_2$ free layer but only slightly degraded for the p-MTJ spin valve with a nanoscale-thick top $Co_2Fe_6B_2$ free layer.

To find out why the i-PMA magnetic moment of the $Co_2Fe_6B_2$ pinned layer and the b.c.c crystallinity of the MgO barrier degraded when the ex situ annealing temperature increased from 350 to 400 °C and why these phenomena are more severe for the p-MTJ spin valve with a nanoscale-thick bottom $Co_2Fe_6B_2$ free layer than for that with a nanoscale-thick top $Co_2Fe_6B_2$ free layer, an atomic compositional depth profile of p-MTJ spin valve was investigated by using secondary ion mass spectroscopy (SIMS), as shown in Fig. 5. For the p-MTJ spin valve with a nanoscale-thick bottom $Co_2Fe_6B_2$ free layer ex situ annealed at 350 °C, the relative Fe concentration of the $Co_2Fe_6B_2$ pinned layer (1169 counts) was higher than that of the $Co_2Fe_6B_2$ free layer (714 counts), as shown in Fig. 5a. Note that the i-PMA magnetic moment of the $Co_2Fe_6B_2$ pinned layer was almost the same as that of the $Co_2Fe_6B_2$ free layer when the 0.4-nm-thick Fe layer was inserted between the $Co_2Fe_6B_2$ pinned layer and the MgO tunneling barrier. This is because the magnetic moment of the $Co_2Fe_6B_2$ free layer sputtered on a b.c.c seed was different from that of the $Co_2Fe_6B_2$ pinned layer sputtered on the MgO tunneling barrier, as shown in Additional file 1: Figure S1. In addition, the Pt atoms of the Pt buffer layer were diffused closely into the MgO tunneling barrier. Otherwise, for the p-MTJ spin valve with a nanoscale-thick top $Co_2Fe_6B_2$ free layer ex situ annealed at 350 °C, the relative Fe concentration of the $Co_2Fe_6B_2$ free layer (1475 counts) was also higher than that of the $Co_2Fe_6B_2$ pinned layer (734 counts) and the Pt atoms of a SyAF layer did not diffuse into the MgO tunneling barrier, as shown in Fig. 5b. Remember that a 0.4-nm-thick Fe layer was always inserted in the MgO tunneling barrier. Thus, the i-PMA magnetic moment of the $Co_2Fe_6B_2$ pinned layer ferro-coupled with the lower SyAF layer for the p-MTJ spin valve with a nanoscale-thick bottom $Co_2Fe_6B_2$ free layer (550 μemu)

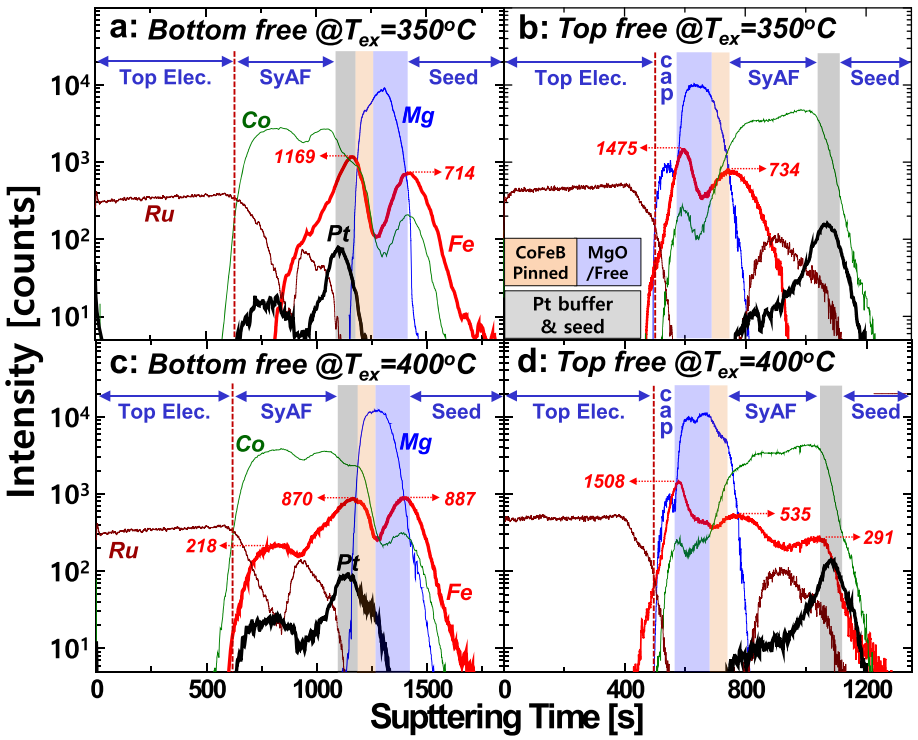

Fig. 5 Dependency of the atomic compositional depth profiles on the p-MTJ spin valve structure and ex situ annealing temperature. **a** p-MTJ spin valve with a nanoscale-thick bottom $Co_2Fe_6B_2$ free layer ex situ annealed at 350 °C, **b** p-MTJ spin valve with a nanoscale-thick top $Co_2Fe_6B_2$ free layer ex situ annealed at 350 °C, **c** p-MTJ spin valve with a nanoscale-thick bottom $Co_2Fe_6B_2$ free layer ex situ annealed at 400 °C, and **d** p-MTJ spin valve with a nanoscale-thick top $Co_2Fe_6B_2$ free layer ex situ annealed at 400 °C

was almost the same as that for the p-MTJ spin valve with a nanoscale-thick top $Co_2Fe_6B_2$ free layer (550 μemu). Considering both the i-PMA magnetic moment of the $Co_2Fe_6B_2$ pinned layer and the crystallinity of the MgO tunneling barrier leads to the TMR ratio for the p-MTJ spin valve with a nanoscale-thick bottom $Co_2Fe_6B_2$ free layer (~160 %) being very slightly higher than that for the p-MTJ spin valve with a nanoscale-thick top $Co_2Fe_6B_2$ free layer (~158 %). Remember that the MgO tunneling barrier for the p-MTJ spin valve with a nanoscale-thick bottom $Co_2Fe_6B_2$ free layer was flat while that for the p-MTJ spin valve with a nanoscale-thick top $Co_2Fe_6B_2$ free layer was flexuous, as shown in Fig. 4a, b. However, for the p-MTJ spin valve with a nanoscale-thick bottom $Co_2Fe_6B_2$ free layer, when the ex situ annealing temperature increased from 350 to 400 °C, the Fe atoms of the $Co_2Fe_6B_2$ pinned layer diffused into the SyAF layer as well as the MgO tunneling barrier, as shown in Fig. 5c. As a result, the Fe concentration of the $Co_2Fe_6B_2$ pinned layer was decreased from 1169 to 870 counts while that of the $Co_2Fe_6B_2$ free layer was increased from 714 to 887 counts, thereby decreasing the i-PMA magnetic moment of the $Co_2Fe_6B_2$ pinned layer ferro-coupled with the lower SyAF layer from 550 to 450 μemu and increasing the i-PMA magnetic moment of the $Co_2Fe_6B_2$ free layer from 85 to 90 μemu, as shown in Fig. 3a, c. In particular, when the ex situ annealing temperature increased from 350 to 400 °C, the Pt atoms of the Pt buffer layer diffused into the MgO tunneling barrier, thereby greatly degrading the b.c.c crystallinity of the MgO tunneling barrier, as shown in Fig. 4a, c. Local f.c.c layers in the MgO tunneling barrier in Fig. 4c evidently originated from the diffusion of the Pt atoms from the Pt buffer layer. Thus, for the p-MTJ spin valve with a nanoscale-thick bottom $Co_2Fe_6B_2$ free layer, when the ex situ annealing temperature increased from 350 to 400 °C, the abrupt TMR ratio decrease from ~160 to ~72 % was obviously associated with both the i-PMA magnetic moment decrease of the $Co_2Fe_6B_2$ pinned layer and the b.c.c crystallinity degradation of the MgO tunneling barrier. Furthermore, for the p-MTJ spin valve with a nanoscale-thick top $Co_2Fe_6B_2$ free layer, when the ex situ annealing temperature increased from 350 to 400 °C, the Fe atoms of the $Co_2Fe_6B_2$ pinned layer also diffused into the SyAF layer as well as the MgO tunneling barrier, as shown in Fig. 5d. As a result, the Fe concentration of the $Co_2Fe_6B_2$ pinned layer was decreased from 734 to 535 counts while that of the $Co_2Fe_6B_2$ free layer was increased from 1475 to 1508 counts, thereby decreasing the i-PMA magnetic moment of the $Co_2Fe_6B_2$ pinned layer ferro-coupled with the lower SyAF layer from 550 to 480 μemu and increasing the i-PMA magnetic moment of the $Co_2Fe_6B_2$ free layer from 82 to 88 μemu, as shown in Fig. 3b, d. In particular, although the ex situ annealing temperature increased from 350 to 400 °C, almost no Pt atoms of a SyAF layer diffuse into the MgO tunneling barrier; thus, a slight b.c.c crystallinity degradation of the MgO tunneling barrier in Fig. 4d would be related to the Fe atom diffusion of the $Co_2Fe_6B_2$ pinned layer rather than the Pt atom diffusion of a SyAF layer. As a result, for the p-MTJ spin valve with a nanoscale-thick top $Co_2Fe_6B_2$ free layer, when the ex situ annealing temperature increased from 350 to 400 °C, the slight TMR ratio decrease from ~158 to ~143 % was evidently associated with both the i-PMA magnetic moment decrease of the $Co_2Fe_6B_2$ pinned layer and the slight b.c.c crystallinity degradation of the MgO tunneling barrier. The atomic compositional depth profile comparison between Fig. 5c and d clearly indicates that the Pt atoms diffusing into the MgO tunneling barrier when the ex situ annealing temperature increased from 350 to 400 °C would be a key factor in the TMR ratio degrading rapidly for the p-MTJ spin valve with a nanoscale-thick bottom $Co_2Fe_6B_2$ free layer (i.e., ~160 to ~72 %) since the Pt atom diffusion into the MgO tunneling barrier intensively degrades the b.c.c crystallinity of the MgO tunneling barrier. In general, it has been reported that Pt has a fast diffusivity and high solubility in metals and inorganic materials [30]. The diffusion distance of Pt atoms during an ex situ annealing depends on solvent material property and the existing strain at the solvent material and Pt layer. In Fig. 5, the diffusion distance of Pt atoms into Ta buffer layer for top $Co_2Fe_6B_2$ free layer structure was longer than that into b.c.c bridge and $Co_2Fe_6B_2$ pinned layer for the bottom $Co_2Fe_6B_2$ free layer structure, which is related to solvent material difference. However, for the top $Co_2Fe_6B_2$ free layer structure, the Pt atoms did not diffuse into the $Co_2Fe_6B_2$ pinned layer since the Pt atoms diffused through the $[Co/Pt]_n$-SyAF layer.

Conclusions

To achieve a higher TMR ratio at the BEOL temperature of 400 °C, i-PMA characteristics (i.e., i-PMA magnetic moment) of both $Co_2Fe_6B_2$ free and pinned layers and the b.c.c crystallinity of the MgO tunneling barrier should be prevented as much as possible from degrading. The design of the p-MTJ spin valve structure is a key to meet these goals. For the p-MTJ spin valve with a nanoscale-thick bottom $Co_2Fe_6B_2$ free layer (Fig. 1a), when the ex situ annealing temperature increased from 350 to 400 °C, the Pt atoms diffused into the MgO tunneling barrier, so the MgO tunneling barrier was transformed from a b.c.c crystallized layer into a mixture layer with local b.c.c, f.c.c crystallized and amorphous layers, thereby abruptly decreasing the TMR ratio because of the much less $\Delta 1$ coherent tunneling of the MgO tunneling barrier. A solution to this issue is a design of the p-MTJ spin valve with a nanoscale-thick top $Co_2Fe_6B_2$ free layer (Fig. 1b) since it could prevent the Pt atoms diffusing into the MgO tunneling barrier

because of non-necessity of a Pt buffer layer (~2.0 nm), resulting in a maximum TMR ratio at the BEOL temperature of 400 °C. In addition, for p-MTJ spin valves, ex situ annealing at the BEOL temperature of 400 °C induces the Fe atoms to diffuse into a SyAF layer, so the i-PMA characteristic (i-PMA magnetic moment) degrades considerably, thereby slightly decreasing the TMR ratio. Thus, further study is necessary to minimize the Fe atom diffusion of the $Co_2Fe_6B_2$ pinned layer for p-MTJ spin valves.

Additional File

Additional file 1: Figure S1. Dependency of the magnetization (M_S*t) and thickness of $Co_2Fe_6B_2$ dead layer (t_{DL}) on the MgO-$Co_2Fe_6B_2$ PMA structure with Fe inserted layer. a PMA structure with single $Co_2Fe_6B_2$ and $Co_2Fe_6B_2$/Fe free layer on Ta seed layer, b PMA structure with single Co2Fe6B2 and Fe/$Co_2Fe_6B_2$ pinned layer on MgO tunneling barrier. (PDF 72.6 KB)

Acknowledgements
This work was supported by a Basic Science Research Program grant from the National Research Foundation of Korea (NRF) funded by the Korean Government (MSIP) (no. 2014R1A2A1A01006474) and the Brain Korea 21 PLUS Program in 2014.

Authors' Contributions
DYL and SEL prepared all the samples, participated in all the measurements and data analysis, and drafted the manuscript. THS and JGP conceived and designed the manuscript. All the authors participated in the data analysis and interpretation of the results. All authors read and approved the final manuscript.

Competing Interests
The authors declare that they have no competing interests.

Received: 28 January 2016 Accepted: 13 September 2016
Published online: 27 September 2016

References
1. Chun KC, Zhao H, Harms JD, Kim TH, Wang JP, Kim CH (2013) A scaling roadmap and performance evaluation of in-plane and perpendicular MTJ based STT-MRAMs for high-density cache memory. IEEE J Solid-st Circ 48:598–610
2. Yoda H, Fujita S, Shimomura N, Kitagawa E, Abe K, Nomura K et al (2012) Progress of STT-MRAM technology and the effect on normally-off computing systems. IEEE Int Electron Devices Meeting 11.3.1-11.3.4. doi:10.1109/IEDM.2012.6479023
3. Park JG, Shim TH, Chae KS, Lee DY, Takemura Y, Lee SE et al (2014) Challenging issues for terra-bit-level perpendicular STT-MRAM. IEEE Int Electron Devices Meeting 19.2.1-19.2.4
4. Ikeda S, Miura K, Yamamoto H, Mizunuma K, Gan HD, Endo M et al (2010) A perpendicular-anisotropy CoFeB–MgO magnetic tunnel junction. Nat Mater 9:721–724
5. Wolf SA, Awschalom DD, Buhrman RA, Daughton JM, Sv M, Roukes ML et al (2001) Spintronics: a spin-based electronics vision for the future. Science 294:1488–1495
6. Amiri PK, Zeng ZM, Upadhyaya P, Rowlands G, Zhao H, Krivorotov IN et al (2011) Low write-energy magnetic tunnel junctions for high-speed spin-transfer-torque MRAM. IEEE Electr Device L 32:57–59
7. Hu G, Topuria T, Rice PM, Jordan-Sweet J, Worledge DC (2013) Optimization of tunneling magnetoresistance in perpendicular magnetic tunnel junctions with Co|Pd reference layers. IEEE Magn Lett 4:3000104. doi:10.1109/IEDM.2014.7047081
8. Lee SE, Shim TH, Park JG (2015) $Co_2Fe_6B_2$/MgO-based perpendicular spintransfer-torque magnetic-tunnel-junction spin-valve without $[Co/Pt]_n$ lower synthetic-antiferromagnetic layer. Nanotechnology 26:475705
9. Yakushiji K, Fukushima A, Kubota H, Konoto M, Yuasa S (2013) Ultralow-voltage spin-transfer switching in perpendicularly magnetized magnetic tunnel junctions with synthetic antiferromagnetic reference layer. Appl Phys Express 6:113006
10. Sato H, Yamanouchi M, Ikeda S, Fukami S, Matsukura F, Ohno H (2013) MgO/CoFeB/Ta/CoFeB/MgO recording structure in magnetic tunnel junctions with perpendicular easy axis. IEEE T Magn 49:4437–4440
11. Yamane K, Higo Y, Uchida H, Nanba Y, Sasaki S, Ohmori H et al (2013) Spin torque switching of perpendicularly magnetized CoFeB-based tunnel junctions with high thermal tolerance. IEEE T Magn 49:4335–4338
12. Chae KS, Park JG (2015) Dependency of tunneling magneto-resistance on Fe insertion-layer thickness in $Co_2Fe_6B_2$/MgO-based magnetic tunneling junctions. J Appl Phys 117:153901
13. Worledge DC, Trouilloud PL (2003) Magnetoresistance measurement of unpatterned magnetic tunnel junction wafers by current-in-plane tunneling. Appl Phys Lett 83:84
14. Lin MS, Lai CH (2007) Perpendicular interlayer coupling through oscillatory Ruderman-Kittel-Kasuya-Yosida interaction between Co/Pt multilayers and Co/Tb Co bilayers. J Appl Phys 101:09D121
15. Miura K, Kimura H, Imanaga S, Hayafuji Y (1992) Magnetic interaction between Co layers and Pd layers in Co/Pd multilayers. J Appl Phys 72:4826
16. Yang HX, Chshiev M, Dieny B, Lee JH, Manchon A, Shin KH (2011) First-principles investigation of the very large perpendicular magnetic anisotropy at Fe|MgO and Co|MgO interfaces. Phys Rev B 84:054401
17. Kim W, Jeong JH, Kim Y, Lim WC, Kim JH, Park JH, et al. Extended scalability of perpendicular STT-MRAM towards sub-20 nm MTJ node. IEEE Int Electron Devices Meeting. 2011;24.1.1-24.1.4. doi:10.1109/IEDM.2011.6131602
18. Karthik SV, Takahashi YK, Ohkubo T, Hono K, Gan HD, Ikeda S et al (2012) Transmission electron microscopy study on the effect of various capping layers on CoFeB/MgO/CoFeB pseudo spin valves annealed at different temperatures. J Appl Phys 111:083922
19. Miyajima T, Ibusuki T, Umehara S, Sato M, Eguchi S, Tsukada M et al (2009) Transmission electron microscopy study on the crystallization and boron distribution of CoFeB/MgO/CoFeB magnetic tunnel junctions with various capping layers. Appl Phys Lett 94:122501
20. Yuasa S, Nagahama T, Fukushima A, Suzuki Y, Ando K (2004) Giant room-temperature magnetoresistance in single-crystal Fe/MgO/Fe magnetic tunnel junctions. Nat Mater 3:868–871
21. Yakushiji K, Noma K, Saruya T, Kubota H, Fukushima A, Nagahama T et al (2010) High magnetoresistance ratio and low resistance–area product in magnetic tunnel junctions with perpendicularly magnetized electrodes. Appl Phys Express 3:053003
22. Lee DY, Shim TH, Park JG (2013) Effects of Pt capping layer on perpendicular magnet anisotropy in pseudo-spin valves of Ta/CoFeB/MgO/CoFeB/Pt magnetic-tunneling junctions. Appl Phys Lett 102:212409
23. Mizunuma K, Ikeda S, Park JH, Yamamoto H, Gan H, Miura K et al (2009) MgO barrier-perpendicular magnetic tunnel junctions with CoFe/Pd multilayers and ferromagnetic insertion layers. Appl Phys Lett 95:232516
24. Zhu Y, Zhang Z, Ma B, Jin QY (2012) Thermal stability of CoFeB/Pt multilayers with perpendicular magnetic anisotropy. J Appl Phys 111:07C106
25. Butler WH, Zhang XG, Schulthess TC, MacLaren JM (2001) Spin-dependent tunneling conductance of Fe|MgO|Fe sandwiches. Phys Rev B 63:054416
26. Khvalkovskiy AV, Apalkov D, Watts S, Chepulskii R, Beach RS, Ong A et al (2013) Basic principles of STT-MRAM cell operation in memory arrays. J Phys D Appl Phys 46:074001
27. Yuasa S, Djayaprawira DD (2007) Giant tunnel magnetoresistance in magnetic tunnel junctions with a crystalline MgO(0 0 1) barrier. J Phys D Appl Phys 40:R337–R354
28. Jeon MS, Chae KS, Lee DY, Takemura Y, Lee SE, Shim TH et al (2015) The dependency of tunnel magnetoresistance ratio on nanoscale thicknesses of $Co_2Fe_6B_2$ free and pinned layers for $Co_2Fe_6B_2$/MgO-based perpendicular-magnetic-tunnel-junctions. Nanoscale 7:8142–8148
29. Takemura Y, Lee DY, Lee SE, Chae KS, Shim TH, Lian G et al (2015) Influence of face-centered-cubic texturing of $Co_2Fe_6B_2$ pinned layer on tunneling magnetoresistance ratio decrease in $Co_2Fe_6B_2$/MgO-based p-MTJ spin valves stacked with a $[Co/Pd]_n$-SyAF layer. Nanotechnology 26:195702
30. Sze SM, Ng KK (2006) Physics of Semiconductor Devices, 3rd edn. Wiley online, p 832, ISBN 978-0-471-14323-9. http://as.wiley.com/WileyCDA/